The Ages of Large Amplitude Coastal Seiches on the Caribbean Coast of Puerto Rico

NORDEN E. HUANG

Engineering Science, California Institute of Technology, Pasadena, California, and Laboratory for Hydrospheric Processes, Oceans and Ice Branch, NASA Goddard Space Flight Center, Greenbelt, Maryland

HSING H. SHIH

NOAA/National Ocean Service, Silver Spring, Maryland

ZHENG SHEN

Engineering Science, California Institute of Technology, Pasadena, California, and Department of Civil and Environmental Engineering, University of California, Irvine, Irvine, California

STEVEN R. LONG

Laboratory for Hydrospheric Processes, Observational Science Branch, NASA GSFC/Wallops Flight Facility, Wallops Island, Virginia

KUANG L. FAN

Institute of Oceanography, National Taiwan University, Taipei, Taiwan

(Manuscript received 3 November 1998, in final form 22 September 1999)

ABSTRACT

Using a process denoted here as the empirical mode decomposition and the Hilbert spectral analysis, the ages of the seiches on the Caribbean coast of Puerto Rico are determined from their dispersion characteristics with respect to time. The ages deduced from this method are less than a day; therefore, the seiches could be locally generated.

1. Introduction

Large amplitude coastal seiches on the Caribbean Coast of Puerto Rico have been observed routinely. The phenomenon has been measured, and the data analyzed by Giese et al. (1990). Later, Chapman and Giese (1990) and Giese and Chapman (1993) have also modeled the generating mechanism of the seiches. They concluded that the seiches are the results of internal waves rushing on the shelf, which then trigger normal modes of the shelf water with the coastal water level change ensuing. Similar phenomena have been observed in many other areas of the world such as Stigebrandt (1976) at Oslo, Norway; Melville and Buchwald (1976) in the Gulf of Carpentaria, Australia; Lamy et al. (1981) in the Gulf of Lions by the Lop-Museum; Giese et al. (1982) and Giese and Hollander (1987) at Palawan Island, the Philippines; Rabinovich and Levyant (1992) near the southern Kuriles; Okihiro et al. (1993) at Barbers Point Harbor, Oahu, Hawaii; Gomis et al. (1993) in the inlets of Balearic Islands; and Giese and Chapman (1998) in the Western Mediterranean Sea. The oscillation covers the amplitude range of water level change from a few tens of centimeters to a few meters, and the period from a few minutes to a couple of hours. Both the amplitude and the period are highly variable depending on the geometry of the water body and the triggering mechanisms. When the geometry is just right, the oscillation can be so severe that the water in a small harbor can be emptied and create great navigation hazards (Giese and Chapman 1993; Okihiro et al. 1993). In this paper, we will use the data from the new tide gauges installed at Magueyes Island, shown in Fig. 1, to determine the source of these seiches through the dispersion relationship. The method we used is the newly developed empirical mode decomposition and the associated Hilbert spectral analysis (Huang et al. 1998).

Corresponding author address: Steven R. Long, NASA GSFC/WFF Code 972, Building n-159, Room W-134, Wallops Island, VA 23337.
E-mail: steve@airsea.wff.nasa.gov

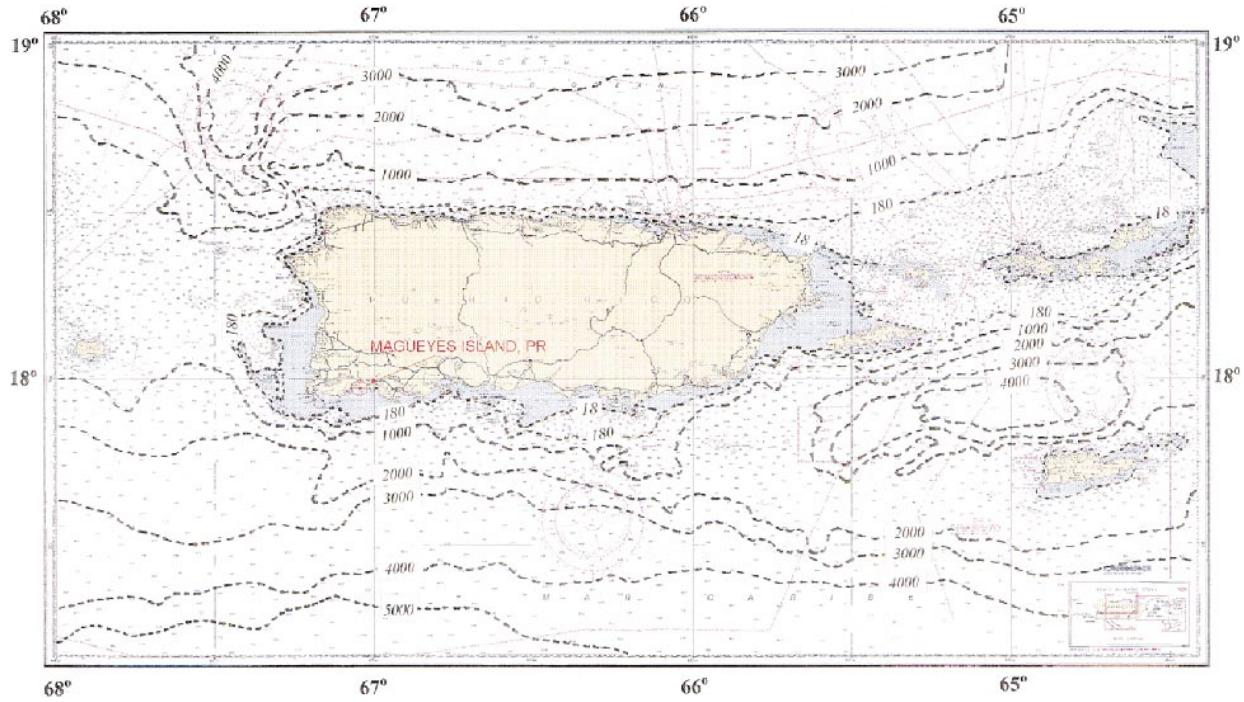

FIG. 1. The geographic location of the Next Generation Water Level Measurement System at Puerto Rico.

2. The new tide gauge and the data

The National Ocean Service (NOS) of the National Oceanic and Atmospheric Administration operates 189 new tide gauges known as the Next Generation Water Level Measurement System (NGWLMS) in the National Water Level Observation Network. The typical installation at these measurement stations is shown in Fig. 2. Basically, the tide measurement apparatus consists of acoustic (primary) and pressure (secondary) water-level sensors as described by Mero and Stoney (1988) and Gill et al. (1995). The primary sensor is capable of sampling at rates of up to four Hertz. It measures water level inside a 1.27-cm sounding tube, which is inside a 15.24- or 30.48-cm protective well. The protective well is used to protect the sounding tube from damage caused by waves and surface debris, and to minimize the temperature and hydrodynamic effects as reported by Shih and Baer (1991) and Porter and Shih (1996). It has a well-to-orifice ratio of 3 and parallel end plates to mitigate flow-induced measurement errors.

The system normally reports tidal information from an average of 181 one-second samples (3-min average) at 6-min intervals. Also reported is the water-level standard deviation of each 3-min record, which was designed for data quality control purposes. Up to 11 ancillary environmental sensors such as wind, temperature, barometric pressure, and humidity can also be connected to the system. Data are transmitted to the central computer facility via NOAA GOES satellites and dedicated telephone lines. A detailed description of the system and capability is given by Mero and Stoney (1988).

Typically, data are relayed to the NOS central office via satellites every three hours. The systems also have the capability of random reporting triggered by tsunami (on the West Coast) or storm surge (on the East Coast) events. The data reporting of these events during the random reporting periods can be set at any desirable intervals. At present the data rate is set at 1 minute and 6 minutes for the tsunami and storm surge, respectively. The data used here, as shown in Fig. 3, were collected at the 6-min rate for five days in September 1994. Although we have conducted an exhaustive search, the only data showing the seiche events are very localized. This is why only five days of data were used here. The water level variation shows typical tidal cycles. Superimposed on the tides are the higher frequency oscillations at the range of 10 cm.

3. Method of data analysis: The Hilbert spectral analysis

Traditionally, the tidal data are analyzed with Fourier-based methods from which only an averaged frequency can be determined. Recently, Huang et al. (1998) have developed a new data analysis method, the empirical mode decomposition (EMD) and Hilbert spectral analysis (HSA). The key part of this approach is the EMD method with which any complicated dataset can be decomposed into a finite and often small number of intrinsic mode functions (IMF). An IMF is defined as any function having the same numbers of zero-crossings and extrema, and also having symmetric envelopes defined

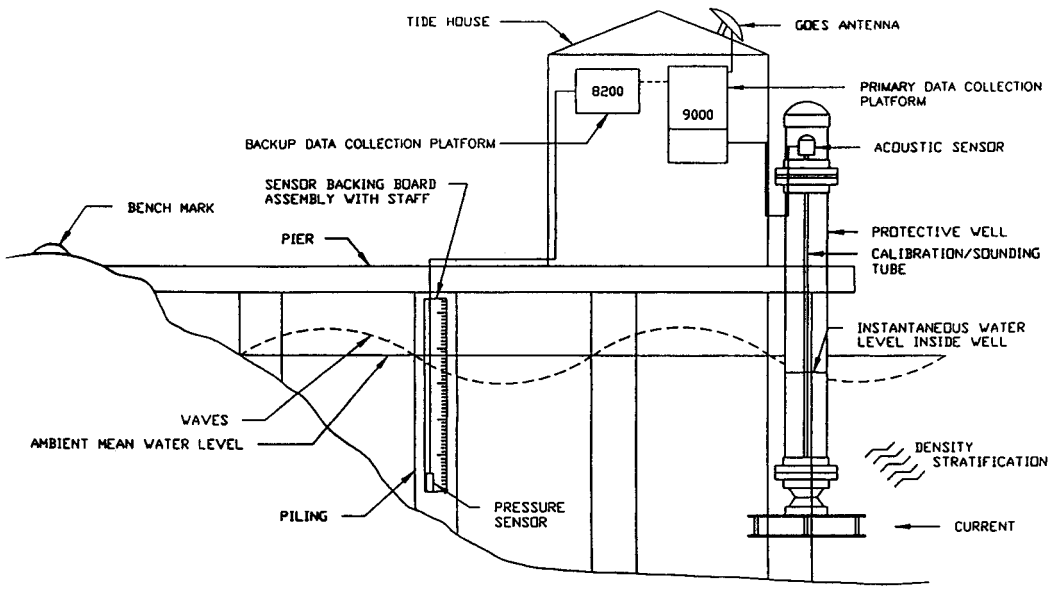

FIG. 2. The schematic diagram of the NOAA NGWLMS.

by the local maxima and minima respectively. The IMF admits well-behaved Hilbert transforms. This decomposition method is adaptive and, therefore, highly efficient. Since the decomposition is based on the local characteristic timescale of the data, it is applicable to nonlinear and nonstationary processes. With the Hilbert transform, the intrinsic mode functions yield instantaneous frequencies by differentiation of the phase function; therefore, the frequency is a function of time, which gives sharp identifications of embedded structures. The final presentation of the results is an energy–frequency–time distribution, designated as the Hilbert spectrum. As the frequency can be defined very precisely, we can use the dispersive properties of the water waves to determine their source as Snodgrass et al. (1966) did for the ocean swell.

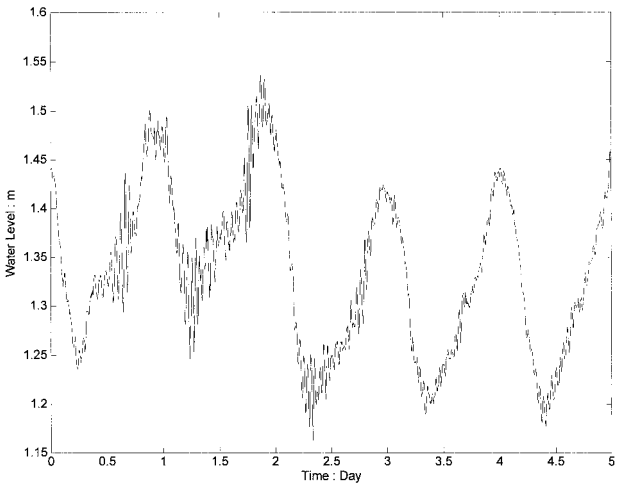

FIG. 3. Selected data from the Puerto Rico tidal station for five days in Sep 1994.

The data were collected by the new NOS tidal system for September 1994. The sampling rate is 1 Hz. When the data is subjected to the EMD method, they give nine components as shown in Fig. 4. The IMF components most noticeable are c6 and c7, which are clearly the semidiurnal and diurnal tides. Yet their amplitude and frequencies are ever changing. This is very different from the Fourier expansion, which would require tens of modes to represent the whole data. With these components, one can reconstruct the original data as follows: In Fig. 5a, we plot the original data in dotted line and the last component, c9, in solid line. The trend of the data is faithfully depicted by the data. Now we will add the components back successively as in Figs. 5b,c. Note in Fig. 5c: the record is dominated by the diurnal tide. Adding the next component, we get the sum as shown in Fig. 5d. At this point, we have practically recovered all the tidal energy. The physical meaning for the next three components are not immediately clear. Fortunately, their magnitudes are all small. When we add all the components up to c2 together, we have the result in Fig. 5f in which the sum up to c3 is given as a solid line and the sum up to c2 as a dotted line. Here the contribution of c2 is clearly illustrated. It essentially represents all the energy in the seiches. When all the components are added back together, we note that all the energy is recovered, as shown for all the cases in Huang et al. (1998).

With this IMF expansion, we can next construct the Hilbert spectrum. In order to show the details of the higher-frequency components, we decided to separate the spectrum into the low (0–5 cycle/day) and the high

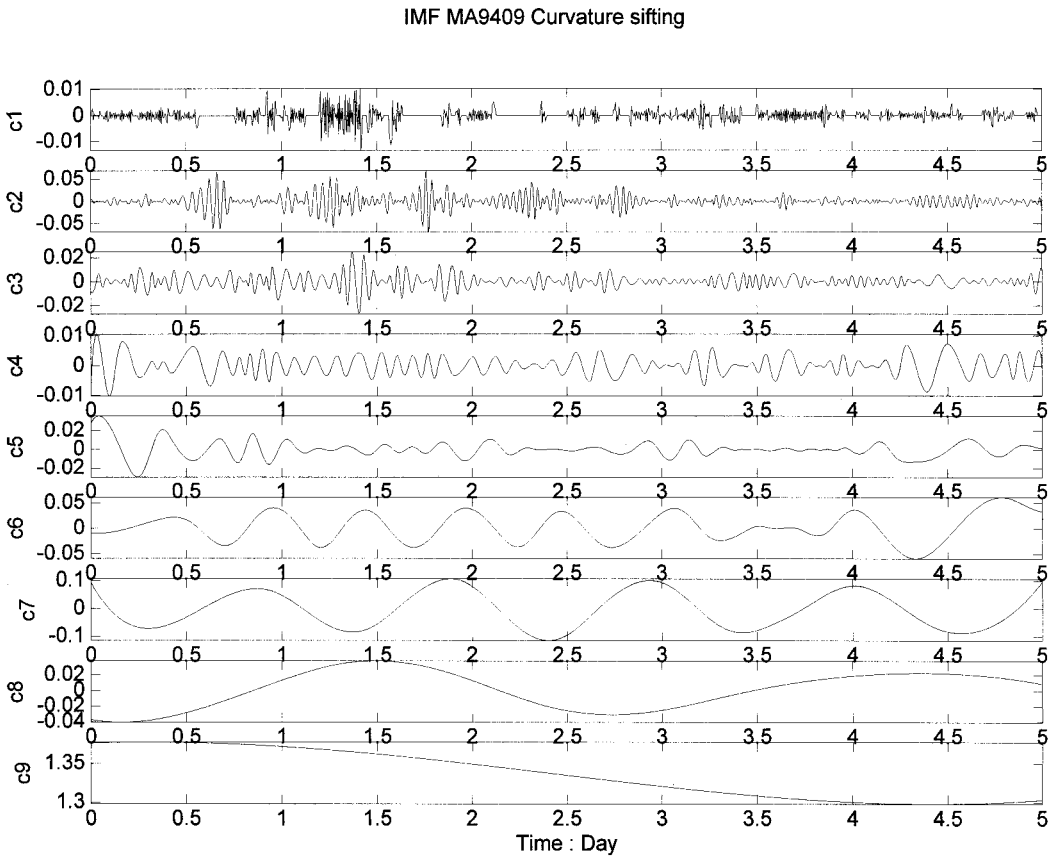

FIG. 4. The intrinsic mode function (IMF) components derived from the data by the empirical mode decomposition method.

(5–60 cycle/day) frequency parts. The low-frequency Morlet wavelet spectrum is shown in Fig. 6, while the corresponding Hilbert spectrum is given in Fig. 7. A detailed calibration of the Hilbert spectrum is given in Huang et al. (1998). Here, both the wavelet and the Hilbert spectrum show a similar time–energy–frequency distribution, but the Hilbert spectrum is more quantitative. There are some end effects showing in the Hilbert spectrum that is inherited from the implementation of the Hilbert transform via the fast Fourier transform routine. Usually, these end effects can be masked by a window, but we did not invoke such a window here. According to both these spectra, the fluctuations of the frequency indicate that the tide is actually nonlinear at the measurement station. This is reasonable, for all the tidal stations are situated in shallow waters. The propagation of the tide over the shallow shelf made their profile nonlinear, even if the generating forces and the governing equations are linear.

The high frequency part of the Hilbert spectrum is given in Fig. 9, while the corresponding Morlet wavelet spectrum is given in Fig. 8. If we integrate the Hilbert spectrum with respect to time, we have the marginal spectrum as shown in Fig. 10 in which we have also plotted the marginal spectrum of the wavelet analysis and the Fourier spectrum, with their magnitude staggered by two decades. Here the comparison should be read with care. To begin with, the marginal spectra do not have the same information content as the full Hilbert or wavelet spectra, for they are merely the projections and not the real substance. Second, the integration of the spectrum with respect to time totally eliminates the time variation. As a result, the advantage of the present method and the wavelet over the Fourier is lost. Even with these understandings, the difference is clear: The smoothly smeared energy contour in the wavelet spectrum was even amplified in this marginal presentation. It really betrays the lack of resolution in the wavelet results as a consequence of the conflicting requirements of localization and frequency resolution or the uncertainty principle. To preserve the localization, the compromise in the Morlet wavelet analysis is to select 5.5 waves in the ''mother'' wavelet. With only 5.5 waves in a window, the frequency resolution is certainly very poor as shown here. The marginal Hilbert spectrum, though not as informative as the full spectrum, still provides a more precise frequency definition than the Fourier spectrum. It indicates that the high-frequency component is in a cleanly cut region around 30 cycle/day, not a smooth but wide peak as in the Fourier spectrum.

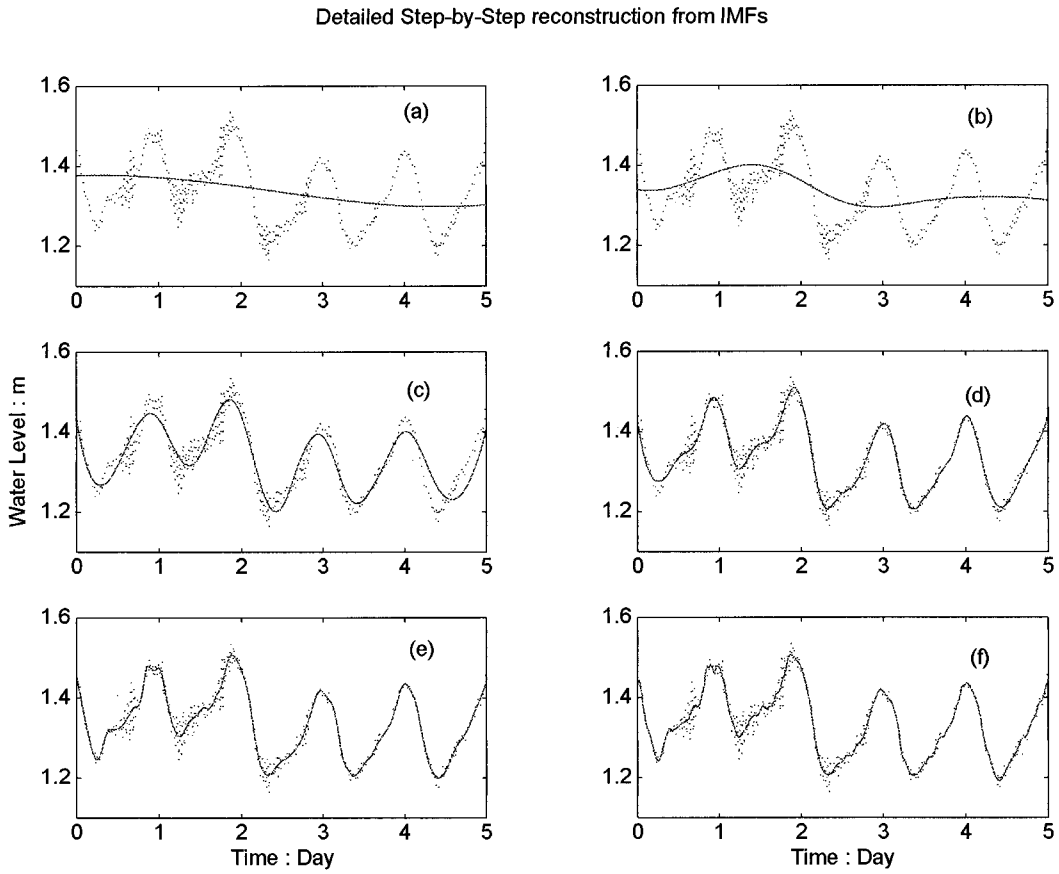

FIG. 5. (a)–(f) The component-by-component reconstruction of the data from the IMF components starting from the lowest frequency components. It is clear in (e) that the tidal oscillation is effectively removed.

Now, let us return to the Hilbert spectrum. In it, we see clear trends of a frequency modulation of the main energy concentration regions on the time axis around the 0.5 and 1.25 day marks. To examine these frequency changes with time, we present two detailed drawings of the Hilbert spectral contour and the IMF component c2 in Figs. 11a and 11b, which represent the main wave packet of the seiche events extracted by the EMD method. In Fig. 11a, the group of waves has their frequency increasing gradually from 21 to 29 cycle/day over the time span of about a quarter of a day. In Fig. 11b, the group of waves near the center of the time span again shows a similar frequency shift. Now we will use this information to determine the source of the seiches.

4. The source of the seiches: Their ages

The age of the seiches can be computed easily from the dispersive properties of the waves as follows. Let us imagine that the propagation of the wave in space along the horizontal axis representing the distance from the source (S) to the measuring station (L), and the vertical axis representing the time. Any waves that initiate from the common source will reach the measuring station at different times according to the dispersive relationship. Therefore,

$$L = c_1 t = c_2(t + \delta t), \tag{1}$$

where the dispersive relationship (see, e.g., Phillips 1977) is given by

$$\sigma^2 = \frac{\delta\rho}{\rho_o} gk[\coth kd + \coth k(D - d)]^{-1}; \tag{2}$$

thus

$$c = \frac{\sigma}{k} = \frac{\delta\rho}{\rho_o}\frac{g}{\sigma}[\coth kd + \coth k(D - d)]^{-1} \tag{3}$$

in which the group velocities of wavenumber 1 and wavenumber 2 are indicated by c_1 and c_2; σ and k are the frequency and wavenumber; $\delta\rho$ and ρ are the density jump and density of the seawater; D and d are the total water depth and the surface layer depth respectively. As the waves are generated at the same place and time but are propagated at different group velocities, they will arrive at different times, at t and $t + \delta t$. Since we do not know the exact density structure of the ocean at the time the event took place, we can only be certain that

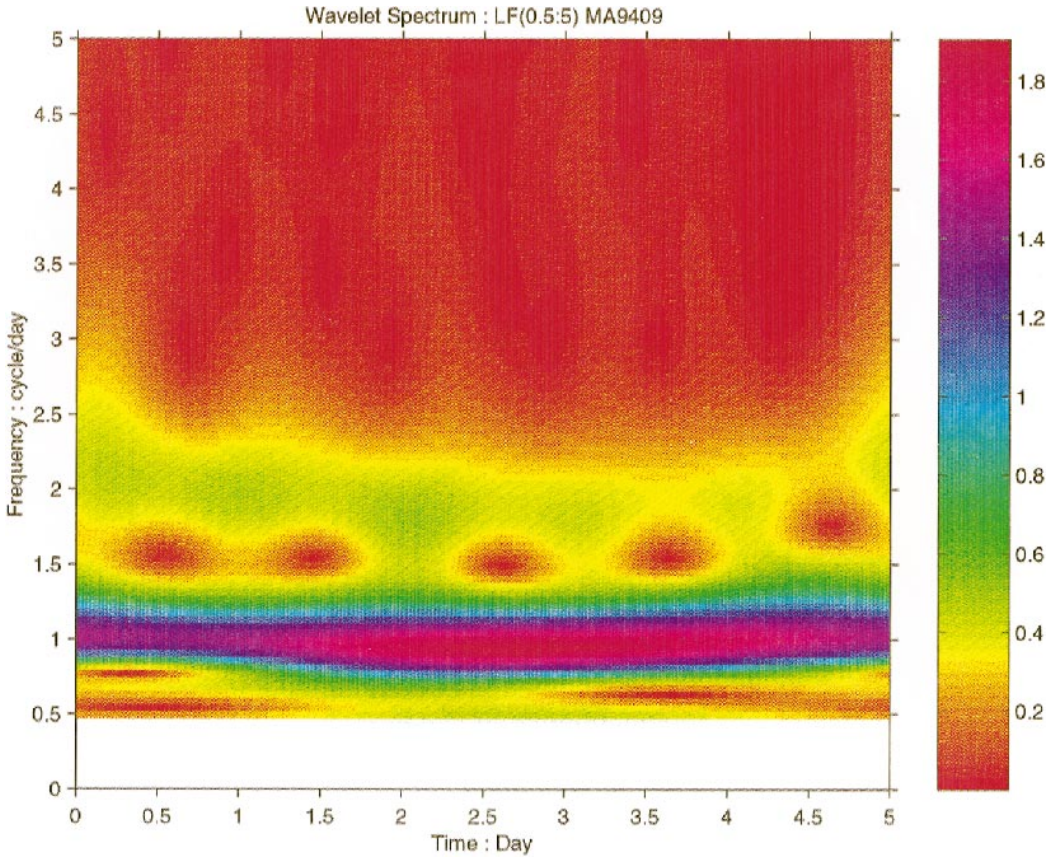

FIG. 6. The low-frequency part of the Morlet wavelet spectrum of the data.

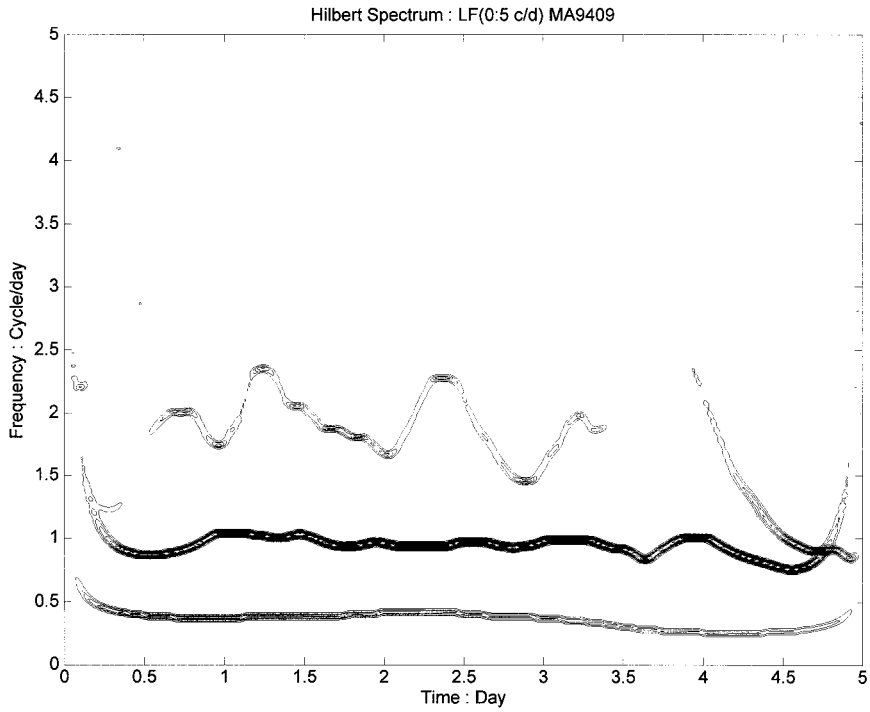

FIG. 7. The low-frequency part of the Hilbert spectrum from the data.

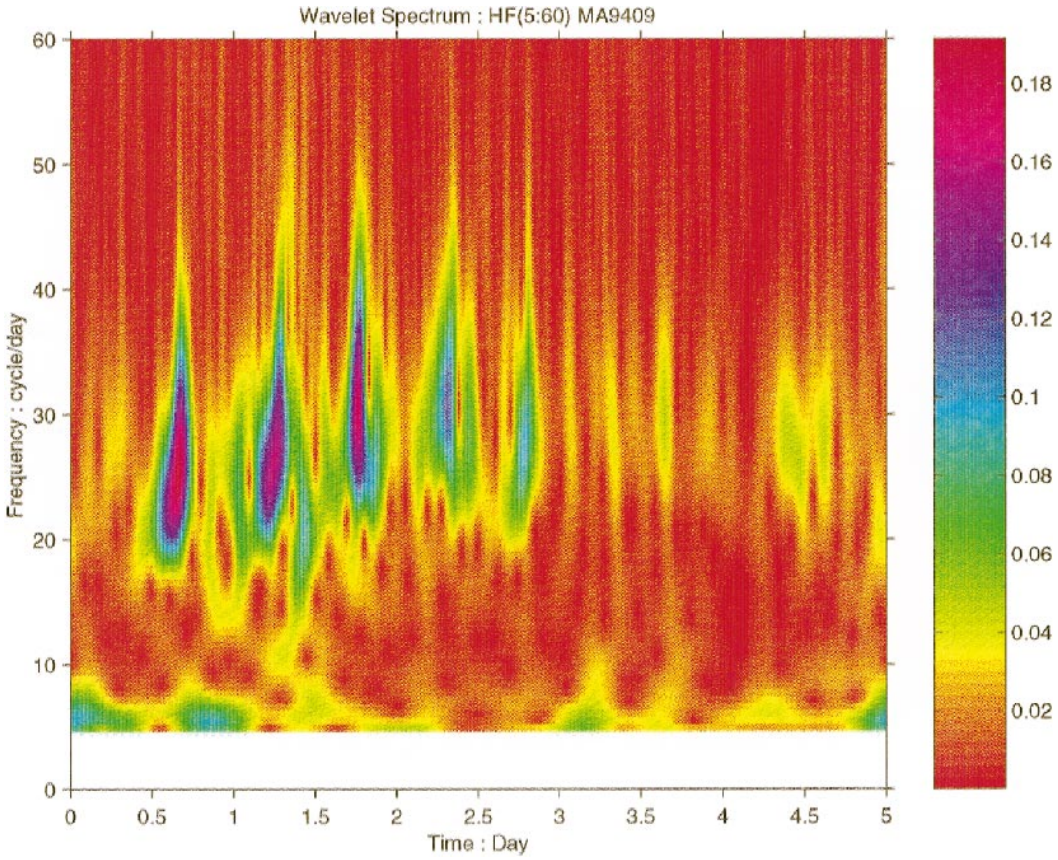

FIG. 8. The high-frequency part of the Morlet wavelet spectrum of the data.

the dispersion relationship given in Eq. (3) describes the group velocity varying inversely with its frequency. Thus,

$$c_1 = \frac{\kappa}{\sigma}, \qquad c_2 = \frac{\kappa}{\sigma + \delta\sigma} \tag{4}$$

in which κ is a function of the density structure of the ocean and the wavenumber. Combining Eqs. (1) and (4), one immediately obtains

$$\frac{\delta t}{t} = \frac{\delta\sigma}{\sigma} \quad \text{or} \quad t = \frac{\delta t\sigma}{\delta\sigma}. \tag{5}$$

Thus we can use the quantitative information gleaned from the Hilbert spectrum to determine the ages of the seiches. This method of using the dispersive properties of the water waves to determine their source was first applied by Snodgrass et al. (1966) for ocean swell. It is a method well founded on the mathematics and physics of wave motions. Based on our best estimate, the ages of the seiches are less than one day. This is very different from the one given by Giese et al. (1990).

The above computation is based on the linear dispersion relationship. As the waves here all appeared in groups, the nonlinear evolution of the groups could be different from that of an infinite train of waves as discussed in Whitham (1975) and Infeld and Rowlands (1990). Let us also discuss the implication of the nonlinear dispersion of the groups. For weakly nonlinear waves as we studied here, the dispersion relationship according to Fornberg and Whitham (1978) should be expressed as

$$\sigma = \sigma_0(k) + \sigma_2(k)a^2 - \frac{1}{2}\sigma_0''(k)\frac{1}{a}\frac{\partial^2 a}{\partial x^2} + \cdots, \tag{6}$$

in which a is the amplitude, $\sigma_2(k)$ is the nonlinear correction to the dispersion relationship, and the prime indicates the derivative with respect to the wavenumber k. With this correction, the dispersion of wavenumber becomes

$$\frac{\partial k}{\partial t} + [\sigma_0'(k) + \sigma_2'(k)a^2]\frac{\partial k}{\partial x} + \sigma_2(k)\frac{\partial a^2}{\partial x} = 0. \tag{7}$$

The evolution of the amplitude becomes the famous nonlinear Schrödinger equation (Infeld and Rowlands 1990). The dispersion of the wave number is then governed by the characteristics of Eq. (5), as

$$\frac{dx}{dt} = \sigma_0'(k) \pm [\sigma_2(k)\sigma_0''(k)]^{1/2}a. \tag{8}$$

Therefore, the dispersion of the group depends critically

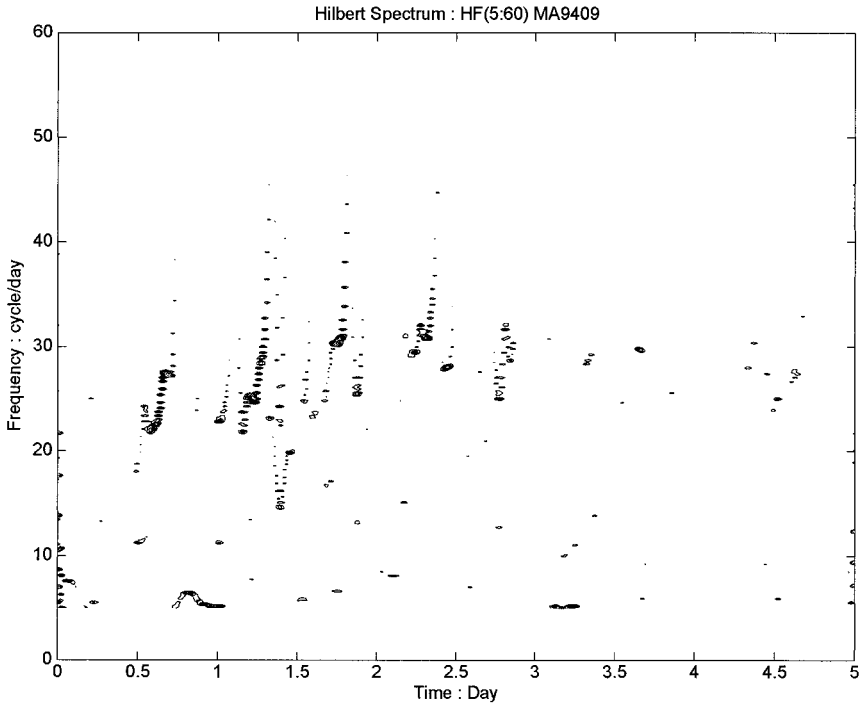

FIG. 9. The high-frequency part of the Hilbert spectrum from the data. Here the increase of frequency with time is clearly visible.

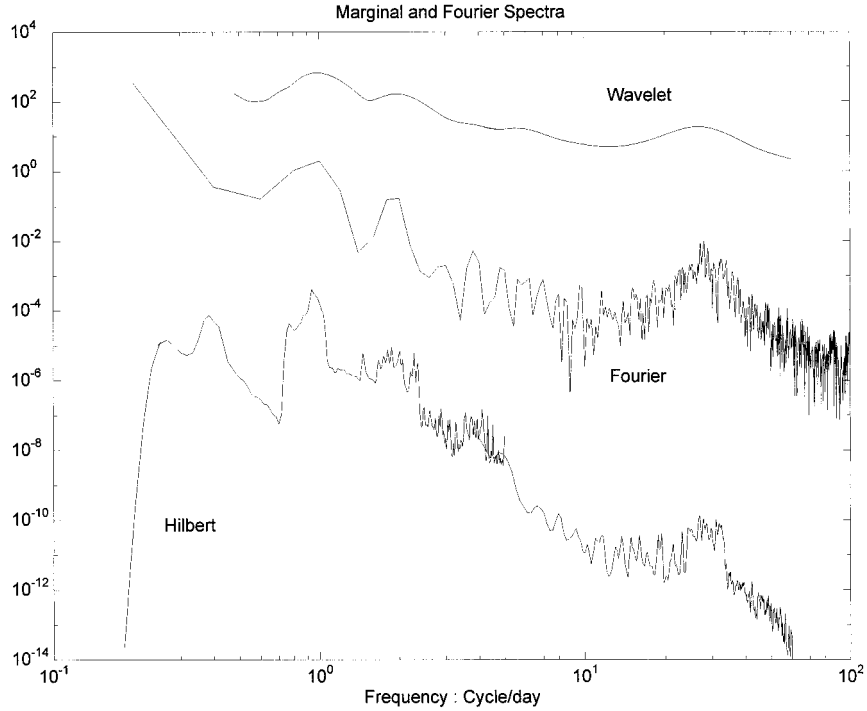

FIG. 10. The marginal Hilbert and wavelet spectra and the Fourier spectrum from the same data. Notice the poor frequency resolution of the Morlet wavelet spectrum, and the poor low-frequency resolution of the Fourier spectrum.

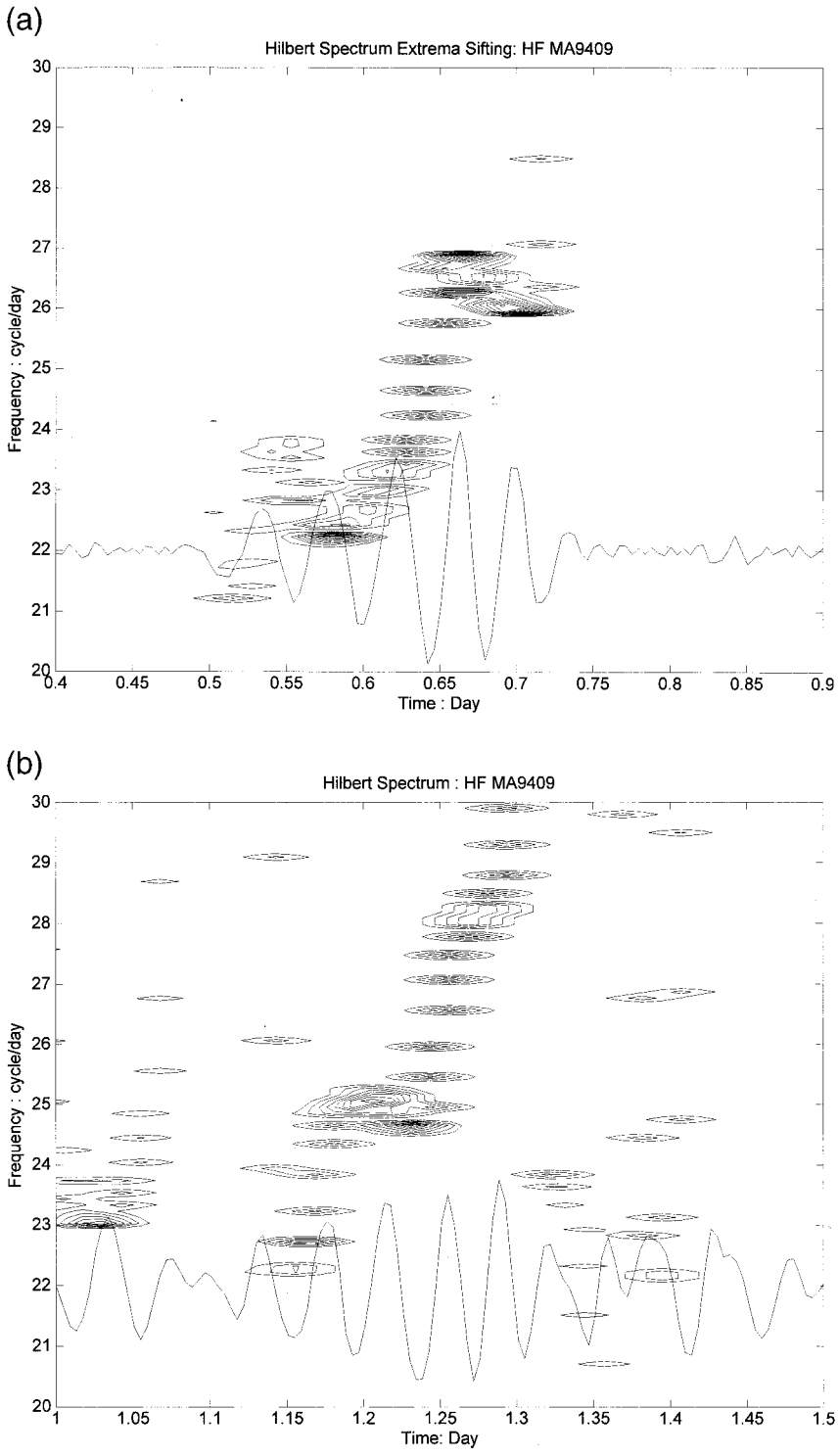

FIG. 11. (a), (b) The detailed presentation of the frequency dispersion of the main energy concentration region together with the corresponding wave packet extracted from the empirical mode decomposition.

on the sign of the nonlinear correction term, $\sigma_2(k)$ and the second derivative of the linear dispersion. For shallow water waves, $\sigma_2\sigma_0'' > 0$; the wave is stable. For deep water waves, $\sigma_2\sigma_0'' < 0$; the wave is unstable. Equation (6) also dictates the integrity of a group; it may split into high and low frequency subgroups. The detailed discussion can be found in both Whitham (1975) and Infeld and Rowlands (1990).

In our case, the group splitting obviously has not happened, for the successive groups all have the same frequency range and distribution. Furthermore, even with the nonlinear corrections, the waves are still dispersive. Therefore, the first-order dispersion is still governed by the linear terms. Thus, we do not have to use the nonlinear dispersion to deduce the age of the wave groups. Consequently, the ages of the seiches cannot be anything older than what we obtained from Eq. (5).

5. Discussion

The causes and the history of coastal seiches and their studies have been ably summarized by Giese and Chapman (1993) and Korgen (1995). Based on these past studies, all the seiches are the results of resonant oscillations in harbors, shelves, straits, bays, and gulfs as the cases may be. The generating mechanisms are either local meteorological disturbances (Meville and Buchwald 1976; Lamy et al. 1981; Gomis et al. 1993) or tides (Stigebrandt 1976).

Giese et al. (1982, 1990), as well as Giese and Hollander (1987), further proposed the generating mechanism as the tidal forces at a remote location that first generated internal waves, which then propagate near the observation station. Thus resonant shelf oscillations are excited that further induce the water level variation observed. Using 10 years of tidal data, they have argued statistically that the seiches mostly occur during the local neap tide and are not related to the local meteorological conditions. Statistically, they also showed that the high seiche activities are about seven days after syzygy. They then argued that only high energy tides have the necessary energy to generate the seiches. As the occurrences of the seiches are all during the neap tide period, they concluded that the source must be so remote that the internal tides will take about seven days to reach the observation station. For the Puerto Rico location, they deduce the generation area of the internal tide to be in the southeastern Caribbean Sea offshore of Venezuela and Trinidad.

In a recent paper by Giese and Chapman (1998), they found that the seiches at Ciutadella Harbor on Menorca Island in the Western Mediterranean Sea also occurs mostly during neap tides. As the Mediterranean Sea is too small to have room for a seven day delay due to wave propagation, they concluded that the neap tide is actually necessary for the generation of seiches. The low tide energy will not introduce strong mixing, therefore, preserving the stratification—a necessary condition for internal tidal wave generation. Can this hypothesis also hold true for Puerto Rico? We believe that it does.

In this study, we used the rigorous dispersion relation to determine the ages of the seiches to be at most one-half day. Using the rough estimated group velocity of 8 km h^{-1} as given by Giese and Chapman (1993), we deduce that the source location cannot be more than 100 km. Over the shallow waters, the phase velocity could be slower, then the generation region could also be closer to the observational station. Local generation was ruled out by Giese and Chapman (1993) strictly based on the statistics of the phase of the tide. In light of their new explanation advanced for the similar phenomena in the Western Mediterranean Sea, we suggest that local generation at Puerto Rico should also be consistent with the observations.

Before ending our discussion, we would like to point out that the wave characteristics studied here are slightly different from that published by Giese et al. (1990) in their appearances. While their waves are definitely of a long train, the waves we studied are in distinct groups. We have searched the NOAA archive, but failed to come up with any record bearing the long wave train data. From the published figures in Giese et al. (1990), the long wave train would suggest a much weaker dispersion than the wave groups found here. This and other discrepancies would require additional studies to resolve. Secondly, the seiches could also be trapped coastal oscillations. The implication of this also needs to be resolved and explored with more detailed data across the shelf in the future. Furthermore, whether there is also interaction of the seiches with the local meteorological forcing should also be studied.

6. Conclusions

Using the newly developed Hilbert spectral analysis, we have examined some selected tidal data at Magueyes Island and found the waves strongly dispersive with respect to time. Based on this dispersion relationship, the ages of the waves cannot be more then one-half day. Therefore, the source location cannot be more than 100 km away. In light of the Giese and Chapman (1998) new study indicating that the seiche could be locally generated, the observed phenomena are consistent with such a local generation scenario: The mechanism is simply that during low tide, the surface layer remains strongly stratified—a necessary condition for internal wave generation. Tides, then, provide the driving force.

Acknowledgments. The authors would like to thank Professor T. Y. Wu for his guidance and advice. This research was completed about a year ago; however, without the encouragement from Graham Giese of Woods Hole, we would not have considered publication. NEH, ZS, and KLF are supported by a grant from NSF (CMS 9615897), NEH is also supported in part by an

ONR grant from the Model and Prediction Program and the NASA RTOP program. ZS is also supported in part through NASA Grant NAG5-5149, and SRL is supported by the NASA RTOP program. KLF also expresses thanks for support from Grant NSC 89-2611-M-002-021.

APPENDIX

The Empirical Mode Decomposition and Hilbert Spectral Analysis

As discussed by Huang et al. (1996, 1998, 1999), the empirical mode decomposition method is necessary to deal with both nonstationary and nonlinear data. Contrary to almost all previous methods, this new method is intuitive, direct, a posteriori, and adaptive, with the basis of the decomposition based on and derived from the data. The decomposition is based on the simple assumption that any data consists of different simple intrinsic modes of oscillations. Thus each mode is designated as an intrinsic mode function with the following definitions:

1) in the whole dataset, the number of extrema and the number of zero-crossings must either equal or differ at most by one, and
2) at any point, the mean value of the envelope defined by the local maxima and the envelope defined by the local minima is zero.

With the definition, one can decompose any function as follows: Identify all the local extrema and then connect all the local maxima by a cubic spline line as the upper envelope. Repeat the procedure for the local minima to produce the lower envelope. The upper and lower envelopes should cover all the data between them. Their mean is designated as m_1, and the difference between the data and m_1 is the first component, h_1 that is,

$$X(t) - m_1 = h_1. \tag{A1}$$

The procedure is illustrated in Huang et al. (1998).

Ideally, h_1 should be an IMF, for the construction of h_1 described above should have made it satisfy all the requirements of an IMF. Yet, even if the fitting is perfect, a gentle hump on a slope can be amplified to become a local extremum in changing the local zero from a rectangular to a curvilinear coordinate system. After the first round of sifting, the hump may become a local maximum. New extrema generated in this way actually recover the proper modes lost in the initial examination. In fact, the sifting process can recover signals representing low amplitude riding waves with repeated siftings.

In the subsequent sifting process, h_1 is treated as the data, then

$$h_1 - m_{11} = h_{11}. \tag{A2}$$

After repeated sifting, up to k times say, h_{1k} becomes an IMF, that is

$$h_{1(k-1)} - m_{1k} = h_{1k}; \tag{A3}$$

then, it is designated as

$$c_1 = h_{1k}, \tag{A4}$$

the first IMF component from the data.

Overall, c_1 should contain the finest scale or the shortest period component of the signal. We can separate c_1 from the rest of the data by

$$X(t) - c_1 = r_1. \tag{A5}$$

Since the residue, r_1, still contains longer period components, it is treated as the new data and subjected to the same sifting process as described above. This procedure can be repeated to obtain all the subsequent r_1, and the result is

$$\begin{aligned} r_1 - c_2 &= r_2, \\ &\vdots \\ r_{n-1} - c_n &= r_n. \end{aligned} \tag{A6}$$

The sifting process can be stopped finally by any of the following predetermined criteria: either when the component c_n or the residue r_n becomes so small that it is less than the predetermined value of substantial consequence, or when the residue r_n becomes a monotonic function from which no more IMF can be extracted. By summing Eqs. (A5) and (A6), we finally obtain

$$X(t) = \sum_{j=1}^{n} c_j + r_n. \tag{A7}$$

Thus, a decomposition of the data into n empirical modes is achieved, with a residue, r_n, which can be either the mean trend or a constant.

We can also use the EMD method as a novel filter. Traditionally, filtering is carried out in frequency space only, but there is a great difficulty in applying the frequency filtering when the data is either nonlinear, nonstationary, or both, for both nonlinear or nonstationary data generate harmonics of all ranges. Therefore, any filtering will eliminate some of the harmonics, which will cause deformation of the data filtered. Using IMF, however, we can devise a time–space filtering. For example, a low-pass filtered result of a signal having n IMF components can be simply expressed as

$$X_{lk}(t) = \sum_{k}^{n} c_j + r_n; \tag{A8}$$

a high-pass result can be expressed as

$$X_{hk}(t) = \sum_{1}^{k} c_j; \tag{A9}$$

and a bandpass result can be expressed as

$$X_{bk}(t) = \sum_{b}^{k} c_j. \tag{A10}$$

The advantage of this time–space filtering is that the

results preserve the full nonlinearity and nonstationarity in the physical space.

Having obtained the intrinsic mode function components, one will have no difficulty in applying the Hilbert transform to each IMF component or in computing the instantaneous frequency by the derivative of the phase function. After performing the Hilbert transform to each IMF component, the original data can be expressed as the real part (RP) in the following form:

$$X(t) = \mathrm{RP} \sum_{j=1}^{n} a_j(t) \exp\left[i \int \omega_j(t)\, dt\right]. \quad \text{(A11)}$$

Equation (A11) gives both amplitude and frequency of each component as functions of time. The same data, if expanded in Fourier representation, would be

$$X(t) = \mathrm{RP} \sum_{j=1}^{\infty} a_j e^{i\omega_j t}, \quad \text{(A12)}$$

with both a_j and ω_j constants. The contrast between Eqs. (A11) and (A12) is clear: The IMF represents a generalized Fourier expansion. The variable amplitude and the instantaneous frequency have not only greatly improved the efficiency of the expansion, but also enabled the expansion to accommodate nonstationary data. This frequency–time distribution of the amplitude is designated as the Hilbert amplitude spectrum, $H(\omega, t)$, or simply Hilbert spectrum. In this instantaneous representation, the nonlinear wave deformation becomes a local frequency modulation rather than the bounded harmonics. Detailed discussion can be found in Huang et al. (1998, 1999).

With the Hilbert spectrum defined, we can also define the marginal spectrum, $h(\omega)$, as

$$h(\omega) = \int_0^T H(\omega, t)\, dt. \quad \text{(A13)}$$

The marginal spectrum offers a measure of total amplitude (or energy) contribution from each frequency value. It represents the cumulated amplitude over the entire data span in a probabilistic sense.

This is a very different approach in representing data in the time–frequency space. The basis used is generated a posteriori, and totally adaptive. As the method is empirical, one cannot exhaust all the possibilities; therefore, average and statistical measures would be impossible, just as in the empirical orthogonal decomposition.

REFERENCES

Chapman, D. C., and G. S. Giese, 1990: A model for the generation of coastal seiches by deep-sea internal waves. *J. Phys. Oceanogr.,* **20,** 1459–1467.

Fornberg, B., and G. B. Whitham, 1978: A numerical and theoretical study of certain nonlinear wave phenomenon. *Philos. Trans. Roy. Soc. London,* **289,** 373–404.

Giese, G. S., and R. B. Hollander, 1987: The relationship between coastal seiches at Palawan Island and tide-generated internal solitary waves in the Sulu Sea. *J. Geophys. Res.,* **92,** 5151–5156.

—— and D. C. Chapman, 1993: Coastal seiches. *Oceanus,* **36,** 38–46.

——, and ——, 1998: Hazardous harbor seiches, tides, wind and baroclinicity. *Ocean Wave Measurements and Analysis,* B. L. Edge and J. M. Hemsley, Eds., Coastal Engineering Research Council of ASCE, ASCE, 208–218.

——, J. F. Fancher, and B. S. Giese, 1982: Evidence of coastal seiche excitation by tide generated internal solitary waves. *Geophys. Res. Lett.,* **9,** 1305–1308.

——, D. C. Chapman, P. G. Black, and J. A. Fornshell, 1990: Causation of large-amplitude coastal seiches on the Caribbean coast of Puerto Rico. *J. Phys. Oceanogr.,* **20,** 1449–1458.

Gill, S. K., and Coauthors, 1995: NOAA/National Ocean Service Platform Harvest Instrumentation. *J. Mar. Geod.,* **18,** 49–67.

Gomis, D., S. Monserrat, and L. Tintore, 1993: Pressure-forced seiches of large amplitude in inlets of the Balearic Islands. *J. Geophys. Res.,* **98,** 14 437–14 445.

Huang, N. E., S. R. Long, and Z. Shen, 1996: The mechanism for frequency downshift in nonlinear wave evolution. *Advances in Applied Mechanics,* Academic Press, 59–118.

——, and Coauthors, 1998: The empirical mode decomposition and Hilbert spectrum for nonlinear and nonstationary time series analysis. *Proc. Roy. Soc. London,* **454A,** 903–995.

——, ——, and ——, 1999: A new view of nonlinear water waves: The Hilbert Spectrum. *Annu. Rev. Fluid Mech.,* **31,** 417–457.

Infeld, E., and G. Rowlands, 1990: *Nonlinear Waves, Solitons and Chaos.* Cambridge University Press, 423 pp.

Korgen, B. J., 1995: Seiches. *Amer. Sci.,* **83,** 330–341.

Lamy, A., C. Millot, and J. M. Molines, 1981: Bottom pressure and sea level measurements in the Gulf of Lions. *J. Phys. Oceanogr.,* **11,** 394–410.

Melville, W. K., and V. T. Buchwald, 1976: Oscillations of the Gulf of Carpentaria. *J. Phys. Oceanogr.,* **6,** 394–398.

Mero, T. N., and W. M. Stoney, 1988: A description of the National Ocean Service next generation water level measurement system. *Proc. Third NOS Int. Hydrographic Conf.,* Baltimore, MD, National Ocean Service, 109–116.

Okihiro, M., R. T. Guza, and R. J. Seymour, 1993: Excitation of seiche observed in a small harbor. *J. Geophys. Res.,* **98,** 18 201–18 211.

Phillips, O. M., 1977: *The Dynamics of the Upper Ocean.* Cambridge University Press, 336 pp.

Porter, D. L., and H. H. Shih, 1996: Investigation of temperature effects on NOAA's next generation water level measurement system. *J. Atmos. Oceanic Technol.,* **13,** 714–725.

Rabinovich, A. B., and A. S. Levyant, 1992: Influence of seiche oscillations on the formation of long-wave spectrum near the coast of the southern Kuriles. *Oceanography,* **32,** 17–23.

Shih, H. H., and L. Baer, 1991: Some errors in tide measurement caused by dynamic environment. *Tidal Hydrodynamics,* B. B. Parker, Ed., John Wiley & Sons, 641–671.

Snodgrass, F. E., G. W. Groves, K. F. Hasselmann, G. R. Miller, W. H. Munk, and W. H. Powers, 1966: Propagation of ocean swell across the Pacific. *Philos. Trans. Roy. Soc. London,* **259,** 431–497.

Stigebrandt, A., 1976: Vertical diffusion driven by internal waves in a sill fjord. *J. Phys. Oceanogr.,* **6,** 486–495.

Whitham, G. B., 1975: *Linear and Nonlinear Waves.* Wiley Interscience, 636 pp.